6-24-2008

Astronomical demonstration of an optical vortex coronagraph

Grover Swartzlander Jr.

Erin Ford

Rukiah Abdul-Malik

Recommended Citation
Optics Express, Optical Society of America, vol. 16, no. 14

Astronomical demonstration of an optical vortex coronagraph

Grover A. Swartzlander, Jr.,[1,*] Erin L. Ford,[1] Rukiah S. Abdul-Malik,[1] Laird M. Close,[2] Mary Anne Peters,[2] David M. Palacios,[3] and Daniel W. Wilson[3]

[1] *College of Optical Sciences, University of Arizona, Tucson, Arizona 85721, USA*
[2] *Steward Observatory, University of Arizona, Tucson, Arizona 85721, USA*
[3] *Jet Propulsion Laboratory, California Institute of Technology, Pasadena, California 91109, USA*
[*] *Corresponding author: grover.swartzlander@gmail.com*

Abstract: Using an optical vortex coronagraph and simple adaptive optics techniques, we have made the first convincing demonstration of an optical vortex coronagraph that is coupled to a star gazing telescope. We suppressed by 97% the primary star of a resolvable binary system, Cor Caroli. The stars had an angular separation of 1.9λ/D at our imaging camera. The secondary star suffered no suppression from the vortex lens.

OCIS codes: (350.1260) Astronomical Optics; (080.4865) Optical Vortices; (110.1080) Adaptive Optics; (110.6770) Telescopes; (070.6110) Spatial Filtering; (120.1880) Detection

References and links

1. A. Wolszczan and D. A. Frail, "A planetary system around the millisecond pulsar PSR1257+12," Nature **355**, 145-147 (1992).
2. G. W. Marcy and R. P. Butler, "Detection of extrasolar giant planets," Annu. Rev. Astron. Astrophys. **36**, 57-97 (1998).
3. S. J. Dick, *The Biological Universe* (Cambridge Univ. Press, Cambridge, 1996).
4. V. G. Ford, P. D. Lisman, S. B. Shaklan, J. T. Trauger, T. Ho, D. Hoppe, and A. E. Lowman, "The Terrestrial Planet Finder coronagraph: technology and mission design studies," Proc. SPIE **5487**, 1274-1283 (2004).
5. D. Coulter, "NASA/s Terrestrial Planet Finder mission: the search for habitable planets," in *Towards other Earths*: *DARWIN/TPF and the Search for Extrasolar Planets*, M. Fridlund and T. Henning, eds., (European Space Agency, 2003), pp. 47-54.
6. A. Karlsson and L. Kaltenegger, "The technology of DARWIN," in *Towards other Earths: DARWIN/TPF and the Search for Extrasolar Planets*, M. Fridlund and T. Henning, eds., (European Space Agency, 2003), pp. 41-46.
7. O. Guyon, E. A. Pluzhnik, M. J. Kuchner, B. Collins, and S. T. Ridgway, "Theoretical limits on extrasolar terrestrial planet detection with coronagraphs," Astrophys. J. Suppl. **167**, 81–99 (2006).
8. O. Guyon, C. Roddier, J. E. Graves, F. Roddier, S. Cuevas, C. Espejo, S. Gonzalez, A. Martinez, G. Bisiacchi, and V. Vuntesmeri, "The Nulling Stellar Coronagraph : Laboratory Tests and Performance Evaluation," PASP **111**, 1321-1330 (1999).
9. R. Galicher, O. Guyon, M. Otsubo, H. Suto, and S. Ridgway, "Laboratory Demonstration and Numerical Simulations of the Phase-Induced Amplitude Apodization," PASP **117**, 411–420 (2005).
10. A. Chakraborty, L. Thompson, and M. Rogosky, "10^{-7} contrast ratio at 4.5λ/D: New results obtained in laboratory experiments using nano-fabricated coronagraph and multi-Gaussian shaped pupil masks," Opt. Express **13**, 2394-2402 (2005).
11. D. Mawet, P. Riaud, J. Baudrand, P. Baudoz, A. Boccaletti, O. Dupuis and D. Rouan, "The four-quadrant phase-mask coronagraph: white light laboratory results with an achromatic device," A&A **448**, 801-808 (2006).
12. J. H. Lee, G. Foo, E. G. Johnson, and G. A. Swartzlander, Jr., "Experimental verification of an Optical Vortex Coronagraph," Phys. Rev. Lett. **97**, 053901(1-4) (2006).
13. J. T. Trauger and W. A. Traub, "A laboratory demonstration of the capability to image an Earth-like extrasolar planet," Nature **446**, 771-773 (2007).
14. K. Enya, L. Abe, S. Tanaka, T. Nakagawa, K. Haze, T. Sato, and T. Wakayama, "High contrast experiment of an AO-free coronagraph with a checkerboard pupil mask," Astron. Astrophys. **480**, 899-903 (2008).
15. M. B. Lyot, "A study of the solar corona and prominences without eclipses," Mon. Not. R. Astron. Soc. **99**, 580 (1939).
16. D. Mawet, P. Riaud, O. Absil, and J. Surdej, "Annular Groove Phase Mask Coronagraph," The Astrophys. J. **633**, 1191 (2005).
17. G. Foo, D. M. Palacios, and G. A. Swartzlander, Jr., "Optical Vortex Coronagraph," Opt. Lett. **30**, 3308-3310 (2005).

#96196 - $15.00 USD Received 14 May 2008; revised 10 Jun 2008; accepted 16 Jun 2008; published 24 Jun 2008

18. S. N. Khonina, V. V. Kotlyar, M. V. Shinkaryev, V. A. Soifer, and G. V. Uspleniev, "The Phase Rotor Filter (PRF)," J. Modern Opt. **39**, 1147-1154 (1992).
19. G. A. Swartzlander, Jr., "Peering into darkness with a vortex spatial filter," Opt. Lett. **26**, 497-499 (2001).
20. G. A. Swartzlander, Jr., "Broadband Nulling of a Vortex Phase Mask," Opt. Lett. **30**, 2876-2878 (2005).
21. G. A. Swartzlander, Jr., E. L. Ford, R. Abdul-Malik, J. Kim, L. Close, M. A. Peters, D, Palacios and D. Wilson, "Advancements of the optical vortex coronagraph," Proc. SPIE **6693,** 669311-17 (2007).
22. M. A. Peters, L. M. Close, M. Rademacher, T. Stalcup, G. A. Swartzlander, E. Ford, and R. S. Abdul-Malik, "A high-Strehl low-resolution optical imager (BESSEL): Detection of a 0.7λ/D separation binary from the ground," New Astron. **13**, 359–369 (2008).
23. B. Kern, T. A. Laurence, C. Martin, and P. E. Dimotakis, "Temporal coherence of individual turbulent patterns in atmospheric seeing," Appl. Opt. **39**, 4879-4885 (2000).
24. G. A. Swartzlander, Jr. "Achromatic optical vortex lens" Opt. Lett. **31**, 2042-2044 (2006).
25. D. W. Wilson, R. E. Muller, P. M. Echternach, and J. P. Backlund, "Electron-beam lithography for micro- and nano-optical applications," Proc. SPIE **5720**, 68-77 (2005).
26. D. W. Wilson, P. D. Maker, R. E. Muller, P. Z. Mouroulis, and J. Backlund, "Recent advances in blazed grating fabrication by electron-beam lithography," Proc. SPIE **5173**, 115-126 (2003).
27. P. D. Maker, D. W. Wilson, and R. E. Muller, "Fabrication and performance of optical interconnect analog phase holograms made by E-beam lithography," Proc. SPIE **CR62**, 415-430 (1996).
28. We acknowledge G. E. Foo, E. Christensen, and G. A. Swartzlander, Jr. for this measurement using the 60" telescope on Mt. Lemmon, Arizona, Dec. 2002. Similar results were later reported in F. Tamburini, G. Anzolin, G. Umbriaco, A. Bianchini, C. Barbieri, "Optical Vortices with Starlight," arXiv:0706.2675v2.
29. J. Burton, "The way I see it. A record of my observations of the night sky: Cor Caroli" x.astrogeek.org/observations/log.php?object_id=508 .
30. R. Dibson-Smith, "The Constellations: Canes Venatici," www.dibonsmith.com/cvn_con.htm .

1. Introduction

Since the early discoveries of planets orbiting distant stars [1,2], and indeed before then [3], astronomers have pondered the possibility, while wrestling with the requirements, of detecting biomarkers from distant worlds [4], e.g., spectral lines of oxygen and water vapor. Current efforts by the U.S. National Aeronautics and Space Administration (the Terrestrial Planet Finder mission) [5] and the European Space Agency (the Darwin mission) [6] to directly detect light from earthlike planets are confounded by the tremendous glare from the parent star. Not only is the planet expected to be roughly 10^7 times less intense that the starlight in the infrared spectrum (10^{10} in the visible), the angular separation is likely to be small for planets in the habitable zone: ~100 mas. One approach to this problem is the development of an ultra-high contrast coronagraph that suppresses starlight while leaving intact the planet light. Various schemes have been proposed, analyzed [7], and tested in the laboratory [8-14]. Reproducing such measurements on a star gazing telescope is challenging, owing in part to atmospheric turbulence, pointing stability, and long integration times. Here we report actual telescope measurements using a promising high contrast imaging instrument, the optical vortex coronagraph (OVC).

Similar in design to a Lyot coronagraph [15] an OVC [16, 17] is able to suppress the glare from a bright point object so that fainter adjacent objects can be better imaged. In contrast to a Lyot coronagraph, which employs an opaque occulting disk to block the central Airy disk, a vortex coronagraph centers the axis of a transparent spiral phase mask (or "vortex lens") with the Airy disk. Both systems employ a "Lyot stop" to remove undesirable diffracted light from the imaging system. A traditional Lyot coronagraph is unsuitable for high contrast imaging because it allows diffract light to bypass the occulting disk and leak through the Lyot stop. In contrast, the OVC takes advantage of the diffractive properties of an optical vortex lens [18-20] having an even valued topological charge, which can diffract all the light outside the Lyot stop. The vortex coronagraph has the potential to completely reject all the light from a point-like star without diminishing light from adjacent objects such as planets, zodiacal dust, or cool stars. Thus far, laboratory measurements have achieved contrast enhancements at an angular separation of $4\lambda/d$ of greater than 10^4 [21]. With improvements in wavefront control and vortex lens fabrication the OVC may be a suitable candidate for a space telescope mission once a contrast of 10^6 is demonstrated. At that value, high performance adaptive optics techniques [13] could be used to obviate scattered light and aberrations, and thus approach the desired 10^{10} contrast value. Many challenges must be surmounted before such values can be

#96196 - $15.00 USD Received 14 May 2008; revised 10 Jun 2008; accepted 16 Jun 2008; published 24 Jun 2008

achieved on a star gazing telescope. Most importantly the star system must have a stationary aberration-free focus on the center of the vortex lens. On Earth that means we must stop the dancing of the stars, which is caused by atmospheric density fluctuations. Techniques now exist to achieve near-stationary astronomical images, thereby affording opportunities to couple OVC's to telescopes, and moreover, advance the development of such systems. We have achieved stationary high Strehl images by use of a small aperture Keplerian telescope and a fast external tip-tilt correcting mirror. When the entrance pupil of the telescope is smaller than the Fried parameter, high speed tip-tilt corrections of the wavefront can deliver a Strehl ratio of roughly 99% [22].

In Section 2 we describe the design of the apparatus. In Section 3 we present our experimental results and numerical analysis. Concluding remarks appear in Section 4.

2. Vortex coronagraph design

A schematic diagram of an optical vortex coronagraph is shown in Fig. 1. The primary star (S_1) is focused on the axis of an optical vortex lens (OVL) whereas the secondary star (S_2) is imaged at a separate point. Spatial filtering of S_1 is achieved by placing an overfilled aperture, i.e., a Lyot stop (LS), in the plane of the exit pupil of the system. Light from this on-axis star is, in principle, completely diffracted outside the exit pupil, whereas off-axis light sources may uniformly fill the exit pupil. The Lyot stop therefore transmits to the imaging camera (Cam_2) only light from S_2. In practice the moving inhomogeneous atmosphere (Atm) severely distorts the wavefronts at the entrance pupil (or aperture, Ap) of the telescope; hence,

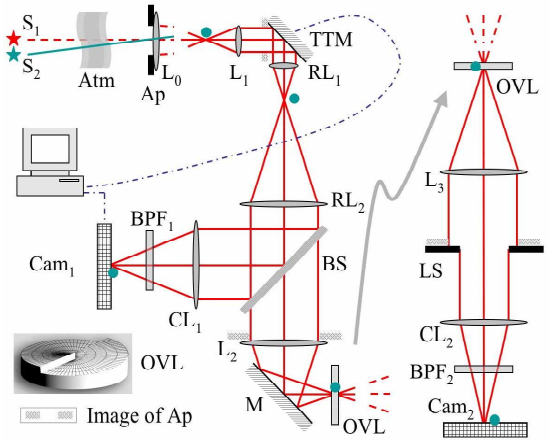

Fig. 1. Schematic diagram showing rays from a binary star system (S_1 and S_2) passing through the atmosphere (Atm) and into a telescope comprised of an objective lens, L_0, and subaperture, Ap. The rays are recollimated by lens L_1 whereby an image of Ap appears at the piezo-electrically driven tip-tilt mirror (TTM). A relay system, RL_1 and RL_2, reproduces this image at the input face of lens L_2. A 50/50 beam splitter (BS) directs light to a fast (500 Hz) camera, Cam_1, whereby the star system is imaged by use of camera lens (CL_1). To correct the wavefront a computer sends a feedback signal to TTM. The remaining light is imaged on the optical vortex lens (OVL) by use of L_2 and recollimated by lens L_3. A Lyot stop (LS) is positioned in the image plane of Ap, and the transmitted light forms a spatially filtered image of the star system on a telescope camera (Cam_2) by use of lens CL_2. Both cameras employ bandpass filters (BPF). The surface of an OVL is illustrated in the inset.

an ideal stationary image of S_1 does not form at the axis of the OVL. Fortunately, the wavefront at the entrance pupil predominantly suffers only tip-tilt distortion when the radius of the entrance pupil, R_{ap}, is less than the Fried parameter, $r_0 \sim 100$ mm. Furthermore, atmospheric fluctuations giving rise to tip-tilt distortion occur on the order of $T_{atm} \sim 0.01$ sec [23]. Using an optical detector and a feed-back system with a response time $\tau << T_{atm}$, one may construct an adaptive optics system that achieves near-perfect seeing when $R_{ap} < r_0$ [23].

#96196 - $15.00 USD Received 14 May 2008; revised 10 Jun 2008; accepted 16 Jun 2008; published 24 Jun 2008

We employed a tip-tiled corrector to stabilize the imaged star system on the optical vortex lens. This was accomplished by forming an image of the entrance pupil on a piezoelectrically driven tip-tilt mirror (TTM). The wavefront was corrected by means of a high speed camera (Cam_1) [Andor iXon EMCCD] and a feedback signal from the camera to TTM [LabView software]. A Pellicle beamsplitter reflects roughly half of the beam to the high speed imaging camera and the remainder is transmitted to a long exposure telescope camera [SBIG ST-402ME]. To ensure that the aperture Ap forms the required image at the lens L_2 (the entrance of the coronagraph system) we found it necessary to insert an optical relay comprised of lenses RL_1 and RL_2. The specifications of our optical elements are listed in Table 1.

Table 1. Optical Design Specifications: diameter, D, focal length, f. Lenses are near-infrared achromatic doublets, except the visible air spaced achromat, L_0.

Element	Ap	L_0	L_1	RL_1	RL_2	CL_1	L_2	OVL	L_3	LS	CL_2
D [mm]	25.4	200	12.7	12.7	25.4	12.7	25.4	2.0	25.4	~ 1.9	12.7
f [mm]		1700	50	25	100	50	100		100		50

The 8-inch refractive finder telescope on the Raymond E. White telescope in the Steward Observatory on the campus of the University of Arizona was used as our objective, L_0. This telescope system is equipped with excellent tracking and "go to" controls. Further, we were able to properly balance the telescope to accommodate our 50 lb system. All other optics had broadband antireflection coatings (including one side of the vortex lens), the surfaces were figured for wavefront errors of $\lambda/10$ or better, and the lenses were achromatic doublets designed for use in the vicinity of 800 nm. The imaging cameras employed bandpass filters, BPF_1 and BPF_2, designed for 800 ± 20 nm. We chose this region of the spectrum owing to a large value of r_0 compared to visible wavelengths, and owing to an absence of strong atmospheric absorption lines, hydroxyl fluorescence lines, and thermal background intensity. A narrow band filter was required because the OVL was chromatic [24]. Both the OVL and LS were mounted on multi-axis translation stages. The optomechanical platform was analyzed for stiffness using professional software [Cosmos SolidWorks]. We calculated a worse case scenario optomechanical error of 0.006 waves at a telescope inclination of 70 deg.

The optical vortex lens was fabricated at the Jet Propulsion Laboratory using analog electron beam lithographic (EBL) techniques [25]. The lens is comprised of spin coated PMMA electron-beam resist on a BK7 glass window having a broadband near infrared antireflective coating and a small 5-arcmin wedge angle to obviate back reflections. Prior to exposure, the PMMA was coated with a 20 nm aluminum discharge layer. A JEOL 9300FS EBL system was then used to expose the OVL dose pattern that was corrected for the nonlinear dose sensitivity of PMMA and the electron-beam proximity effect. After exposure, the aluminum discharge layer was removed in aqueous base developer, and the PMMA was developed using acetone in an iterative manner until the desired depth was achieved.

The fabricated OVL surface quality was measured with a phase shifting interferometric profilometer [Veeco NT 9800]. The central region near the vortex axis, shown in Fig. 2(a), is relatively smooth. In comparison, the zoomed out image in Fig. 2(b) reveals surface errors near the electron beam field boundaries. In an attempt to minimize the apparent dose non-uniformity, a two-pass exposure was performed using field sizes of 300 μm and 400 μm square, with the vortex core positioned at the midpoints of the central fields. The cause of the field boundary non-uniformity is under investigation. It is significantly worse than was observe in other analog diffractive optics fabricated by EBL such as blazed gratings [25, 26] and computer-generated holograms [27]. Resist heating [25] or residual charging of the non-conductive substrate by the higher energy beam may be the cause.

Atomic force microscope measurements in the vicinity of the vortex core indicate that the surface pitch is $\Delta d = 1.661$ μm. Assuming the refractive index of PMMA is 1.486, the "design" wavelength λ_0 at which the doubly pitched surface produces a vortex of topological

#96196 - $15.00 USD Received 14 May 2008; revised 10 Jun 2008; accepted 16 Jun 2008; published 24 Jun 2008

charge $m(\lambda_0) = 2.0$ is $\lambda_0 = (\Delta d)(n_{PMMA}-1) = 807$ nm [17]. The topological charge at other wavelengths is given by $m(\lambda) = m(\lambda_0)\lambda_0/\lambda$. At the wavelength corresponding to the center of the bandpass filter the topological charge is therefore expected to be $m(\lambda) = 2.02 \pm 0.05$.

The surface roughness over the central patch of the vortex lens may be characterized by the standard deviation in the height, σ_h. Using a Veeco profilometer we determined that σ_h is equivalent to $5/1000^{th}$ of a wave (at the design wavelength). This error is small in comparison to the 3.5% topological charge error owing to the bandwidth and mismatch of our bandpass filter. However, the lithographic stitching errors produced undesirable surface deviations of 2 to 5%. The rectilinear pattern of the latter may diffract unwanted light from the on-axis star through the Lyot stop and therefore degrade the device performance.

The rectangular dimensions of the vortex lens are 2 mm x 2 mm. According to the values in Table 1 the re-imaged pupil at lens L_2 has a diameter of D_2=3.0 mm. Hence, the diameter of the focal spot on the vortex lens has a calculated value of 65 μm. As evident from an examination of Fig. 2(a), this focal spot falls within a single e-beam writing patch on the fabricated vortex lens. Any light from the primary star that is scattered from the e-beam stitching errors can therefore be attributed to light from the outer Airy rings, not from the central Airy disk. The area of the vortex lens accommodates roughly 37.5 complete Airy rings across its surface. The secondary star lays 19.3 arcsec from the primary, which corresponds to $2.99\lambda/D_2$ at the vortex lens, where $\lambda/D_2 = 267$ μrad = 55 arcsec. This angular separation is equivalent to 79.6 μm on the vortex lens. Therefore, the image of the secondary star on the vortex lens is expected to appear in the second Airy ring of the primary star. The close proximity of these two bodies constitutes a small inner working angle and is a challenging regime for a high contrast coronagraph.

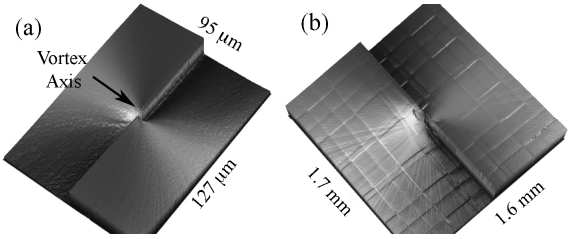

Fig. 2. Surface profile of the optical vortex lens in PMMA resist showing (a) relatively good surface quality in the central region containing the vortex axis, and (b) significant surface roughness owing to exposure non-uniformity near electron-beam field boundaries.

3. Experimental results

Earlier experiments on a large aperture (60-inch diameter) demonstrated the need to minimize the effects of poor atmospheric seeing [28]. In most camera exposures the star focused well away from the vortex axis. A rare case where the two coincided is shown in Fig. 3(a). This finding demonstrated the need to apply adaptive optics techniques to the OVC. For comparison, an image of a star using our high Strehl vortex coronagraph is shown in Fig. 3(b).

Before testing the nulling capacity of the OVC on a binary star system we tested the system in the laboratory using a fiber-coupled diode laser as a coherent light source. Without the vortex lens in place we obtained a high Strehl image showing many Airy rings, as seen in Fig. 4(a). With the vortex lens in place the central Airy disk assumed a ring profile, as shown

#96196 - $15.00 USD Received 14 May 2008; revised 10 Jun 2008; accepted 16 Jun 2008; published 24 Jun 2008

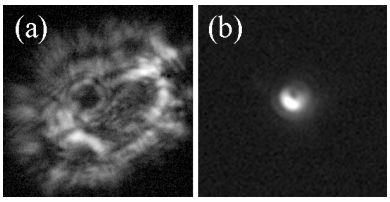

Fig. 3. (a). Image of a star (Betelgeuse) through a vortex lens without adaptive optics [28]. (b) Image of a star (Arcturus) through a vortex lens using adaptive optics.

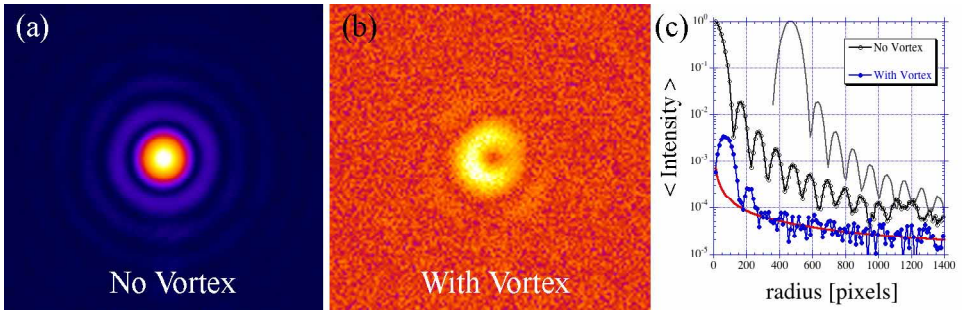

Fig. 4. False color laboratory measurements using a vortex coronagraph. (a) Without vortex lens. (b) With vortex lens. (c) Radially averaged intensity profiles of the data in (a) and (b). Black solid curve in (c) shifted to 4λ/D.

in Fig. 4(b). Relative to the peak of the Airy disk, the vortex lens suppressed the center peak by a factor of ~1/400 (~99.8%), and the average maximum value of the ring was 200 times smaller. More importantly, the contrast at the fourth Airy ring (see shifted line) corresponds to a contrast of 2.3×10^{4}, as is evident by the azimuthally averaged plots in Fig. 4(c).

To test the nulling capability of the OVC when it is coupled to a star gazing telescope, we pointed the telescope at the binary star system, Cor Caroli (alf 2 CVn) in the constellation Canes Venatici. The stars have a known separation of 19.3 arcsec and have a visible magnitude difference of ΔM=2.7 (i.e., 12 times flux ratio), with the primary star having a magnitude of 5.6. It is an infrared source and is 110 light years from Earth. The primary star is a variable star with visual amplitude change of up to 0.1 [29]. The primary is labeled a^2 or $alpha^2$ since it is slightly east of its companion a^1 or $alpha^1$ [30].

We recorded images and dark frames at 300 second exposures through an 800 nm ± 20 nm bandpass spectral filter. When the vortex lens was significantly misaligned, the strong primary (a^2) and the weak secondary (a^1) stars are resolved in Fig. 5(a). This false color image is unaltered data from which a dark frame image has been subtracted. The absence of Airy rings around the stars suggests our system was slightly defocused. This suggestion is supported by our numerical analysis of the defocused point spread function (see below).

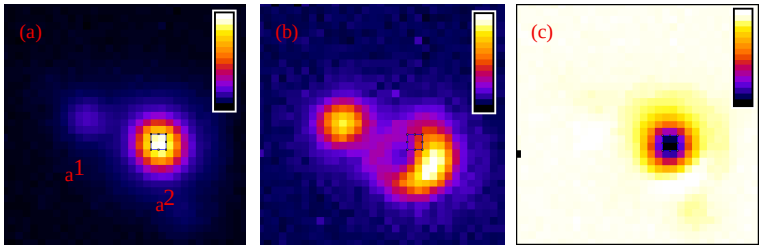

Fig. 5. Raw dark-frame-subtracted images of Cor Caroli in false color (a) without vortex, (b) with vortex, (c) difference with (a) subtracted from (b). The 2x2 pixel outline in each image demarks the registration position that produces the greatest difference.

#96196 - $15.00 USD Received 14 May 2008; revised 10 Jun 2008; accepted 16 Jun 2008; published 24 Jun 2008

After adjusting the vortex axis with the primary star, the relative magnitudes of both stars were rendered nearly equal, as can be seen in Fig. 5(b). The difference between Fig. 5(a) and (b), shown in Fig. 5(c), suggests that the signal from the secondary star is nearly unaffected by the vortex lens, whereas the primary starlight is suppressed. The offset between the dark hole and the 2x2 pixel outline in Fig. 5(b) suggests the vortex axis was slightly misaligned.

Using a Fourier interpolation technique (zero padding in the transformed domain), we obtained a clearer impression of the recorded images, as shown in Fig. 6. This interpolation affords an ability to make calculations and line plots with less pixelation noise. High spatial frequency noise has been numerically filtered from the images by use of a super-Gaussian soft aperture. These images allowed us to plot the intensity profiles shown in Fig. 6(d). The black (blue) line corresponds to the intensity without (with) the vortex aligned with the primary star. Each of the plots corresponds to the same line of points in the images. This data was selected by tracing a line segment through the peaks in Fig. 6(a). Without the vortex lens the "uncorrected" intensity peak of the primary (secondary) star has a value of 467.57 (73.39) in arbitrary units. The dark floor for this case was found to be 9.75±0.41. We note that the ratio of the corrected peaks (measured at 800 nm) is equal to 457.8/63.6 = 7.2 (or ΔM=2.14), which is less than the reported value in the visible spectrum (12.1). After introducing the vortex lens (see Fig. 6(b)) the uncorrected peak value of the primary (secondary) star is 84.20 (73.73), with a dark floor of 7.67±0.32. Here we are concerned with the maximum suppression afforded by the vortex lens. Subtracting the dark floor from both signals, we calculate the point-by-point percent change, shown in Fig. 6(c). We find the maximum percent change is 97%, as indicated by the black hole in Fig. 6(c) and the red line in Fig. 7.

Using the data from Fig. 6(a) we were also able to match the measured intensity profile of each star with a defocused point spread function, as shown by the dashed lines in Fig. 6(d). The good agreement between the measured and calculated distributions suggests that the imaging optics were slightly defocused. The non-optimal performance of the OVC indicates that aberrations are introduced by the telescope objective or the relay system.

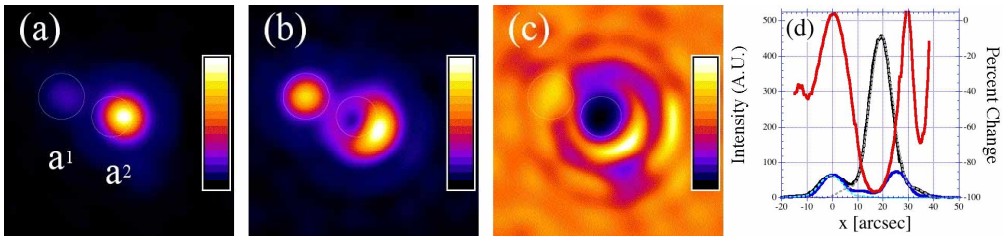

Fig. 6. Interpolated images (a) without vortex (f_a), (b) with vortex lens (f_b), (c) Relative difference, $(f_b-f_a)/f_a$. (d) Black line: Intensity plot through the peaks of the primary and secondary star without the vortex lens. Blue line: Same points with the vortex lens. Red line: the percent change that reaches -97%. Dashed lines: computer generated defocused point spread functions.

Although the AO system corrects for tip and tilt wavefront fluctuations, the performance of the coronagraph is vulnerable to higher order phase distortions. By numerically including a quartic phase variation ranging from 0 to π across the entrance face of L_2, and by including a small displacement of the vortex lens from its optimum position (1/3 the radius of the Airy disk), we were able to qualitatively reproduce in Fig. 7 the experimentally obtained images in Fig. 6. The computed binary system having no coronagraphic filtering is shown in Fig. 7(a). The corresponding vortex coronagraph image is shown in Fig. 7(b). The agreement with the respective images in Fig. 6 is remarkably good, up to an inconsequential orientation angle. For comparison we depict the corresponding image for a traditional Lyot coronagraph in Fig. 7(c). In the latter case we assumed the occulting disk blocks the entire central Airy disk of the focused beam. This shows that in the face of modest higher order wavefront distortion the vortex coronagraph is at least as effective as the Lyot coronagraph. With no wavefront

#96196 - $15.00 USD Received 14 May 2008; revised 10 Jun 2008; accepted 16 Jun 2008; published 24 Jun 2008

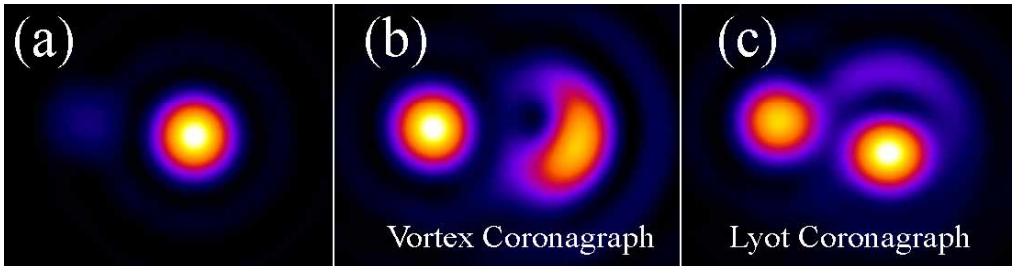

Fig. 7. Numerically generated images (a) without (b) with the vortex lens. To achieve agreement with the experimental images (see Fig. 6) quartic wavefront distortion at the telescope objective was included, and the vortex lens was misaligned. (c) Predicted image for the same system using instead, a Lyot coronagraph with the central Airy disk occulted.

distortion, and with the star centered on the vortex lens, the right-most star in Fig. 7(b) disappears, resulting in the complete suppression of the primary star (not shown).

4. Conclusion

We have constructed and mounted to a telescope an optical vortex coronagraph coupled to a tip-tilt correcting adaptive optics system. The latter was designed to produce a Strehl ratio of ~99%, and to maintain a stationary focus on an optical vortex lens. Images of a binary star system with an effective angular separation of $1.9\lambda/D$ were recorded with and without the vortex lens in place. The intensity of the primary star was suppressed by 97% whereas the intensity of the secondary star was unaffected. In comparison, the system achieved a suppression of 99.8% in the laboratory. We attribute the difference to systematic and human errors, e.g., wavefront distortion from optical elements and misaligned optics. A larger telescope aperture or lower noise cameras would help overcome dark noise limitations. At an angular separation of $4\lambda/d$ our laboratory measurements achieved a contrast of 2×10^{4}. Improving the suppression of the primary starlight at angles of zero and $4\lambda/d$ will require the fabrication of a higher quality vortex lens. Inasmuch as the performance of the OVC is limited by the quality of the incident wave, future work will include a means to verify that the incident beam is indeed planar and uniform. Future telescope measurements will include improved optomechanical systems for optimizing the alignment, and the inclusion of advanced adaptive optics techniques to mitigate wavefront errors. With such advances, we believe the optical vortex coronagraph will be a suitable candidate for a space telescope mission to directly observe earthlike exoplanets.

Acknowledgments

We gratefully acknowledge assistance from Roger Ceragioli, Tom Fleming, Dave Harvey, Chris Limbach, Joshua Nelson, and Gary Rosenbaum (Steward Observatory), and Joshua Kim (College of Optical Sciences) at the University of Arizona. We are also grateful for comments from Stewart B. Shaklan and Wesley Traub (Jet Propulsion Laboratory, California Institute of Technology), and Olivier Guyon (Subaru Telescope, National Astronomical Observatory of Japan). We thank Joanna Schmit (Veeco Inc., Metrology Group, Tucson, AZ) for profilometric measurements. We acknowledge earlier vortex coronagraph collaborations with Gregory E. Foo (Northrop Grumman Space Technology, Long Beach, CA) and Eric Christensen (Lunar and Planetary Laboratory, University of Arizona). The U.S. Army Research Office, the U.S. Air Force Office of Scientific Research, and the Jet Propulsion Laboratory supported the effort in the College of Optical Sciences. The Steward Observatory effort was supported by NASA Origins and the National Science Foundation Career program. The Jet Propulsion Laboratory effort was supported under contract with the National Aeronautics and Space Administration (NASA).

#96196 - $15.00 USD Received 14 May 2008; revised 10 Jun 2008; accepted 16 Jun 2008; published 24 Jun 2008